Journal of Chromatography A 1758 (2025) 466219

Contents lists available at ScienceDirect

Journal of Chromatography A

journal homepage: www.elsevier.com/locate/chroma

Separation of empty and full adeno-associated viral capsids by MCSGP: From model-based design to implementation

Luca Ossi [a], Helena Marie [b], Michael Schulte [b], Mattia Sponchioni [a,*]

[a] Department of Chemistry, Materials and Chemical Engineering, Politecnico di Milano, Via Mancinelli 7, Milano, 20131, Italy
[b] Merck Life Science KGaA, Frankfurter Str. 250, Darmstadt, 64293, Germany

ARTICLE INFO

Keywords:
AAVs
Empty/full separation
Chromatography
Ion exchange
MCSGP

ABSTRACT

Adeno-associated viruses (AAVs) are acquiring growing importance in the gene therapy scenario. However, an efficient separation of particles enveloping the desired genetic cargo, known as full AAVs, from empty or misloaded particles is yet to be achieved. In this work, we systematically investigated the empty/full separation for AAV2 by anion exchange chromatography. First, the role of the gradient slope and salt concentration in the wash and equilibration stages were elucidated in single-column operations. Then, a model-based optimization algorithm was developed to establish the most effective combinations of these parameters to maximize yield and productivity at a given purity specification (Pspec). We demonstrated that a tradeoff is in place. In fact, the yield could be maximized to 11.3 % (for Pspec=70.0 %) when increasing the gradient duration to 30 column volumes (CV), which led to a decrease in the productivity to 3.28E13 viral particles per liter of resin per hour (VP/(L_{resin} h)). On the other side, with a 20 CV gradient, the productivity improved to 3.85E13 VP/(L_{resin} h), but the yield correspondingly decreased to 10.2 % This tradeoff could be alleviated by adopting the multicolumn countercurrent solvent gradient purification (MCSGP). After having highlighted the operability region of MCSGP, defined through model simulations, an experimental run allowed us to obtain simultaneously high yield (57.8 %) and productivity up to 8.65E13 VP/(L_{resin} h) when targeting the same Pspec=70.0 %, greatly improving the batch performance. At the same time, the process mass intensity could be cut by a factor 3, thus demonstrating the potential of this twin-column process in the empty/full AAV separation.

1. Introduction

Adeno-associated viruses (AAVs) are attracting growing attention as gene delivery vectors [1,2]. The proteinaceous capsids of these viruses can, in fact, efficiently pack the transgene of interest preventing its premature degradation by the serum endonucleases and favor its penetration of the cell barrier [3–6]. These features, coupled with their low immunogenicity to humans, make AAVs fascinating carriers for gene therapies, currently investigated for complex and rare diseases like hemophilia, spinal muscular atrophy, cystic fibrosis, and neurodegenerative conditions [7,8]. Among the different possible serotypes, bearing specific capsid proteins and tropism for the target cells, AAV2 currently represents the most investigated one for the treatment of human diseases [9].

So far, only five gene therapy products based on AAVs received market authorization by the Food and Drug Administration, namely Zolgensma, Luxturna, Elevidys, Hemgenix, and Roctavian [10]. However, since many more are in the pipeline, having demonstrated good results in phases I and II clinical trials, we may expect an important increase in their demand in the coming years. This requires efficient manufacturing processes, able to deliver pure and safe AAVs at affordable costs for the patients.

The biomanufacturing through transient transfection of a mammalian cell line, most often the human embryonic kidney cells HEK293, is reported to stably produce AAVs in good titer [11,12]. However, the target entities, represented by the viral capsids packing the full-size transgene of interest, often referred to as full AAVs, are produced together with a variety of impurities. Among them, the most critical to handle is represented by empty capsids. These, although not bearing specific side-effects, do not contribute to the therapeutic outcome of the AAV-based formulation, while instead actively triggering the human immune response and competing with full capsids for the same receptor sites [13–15]. The separation of these product-related impurities and consequent enrichment of the formulation in full particles is therefore a

* Corresponding author.
E-mail address: mattia.sponchioni@polimi.it (M. Sponchioni).

https://doi.org/10.1016/j.chroma.2025.466219
Received 18 April 2025; Received in revised form 30 June 2025; Accepted 10 July 2025
Available online 11 July 2025

critical task of the downstream processing. At the same time, the very similar physicochemical properties between empty and full AAVs make this separation particularly challenging.

One of the most employed processes used for this enrichment is ultracentrifugation, leveraging the difference in Buoyant density between empty and full particles [16–20]. Despite it allows achieving good resolution, it brings about important scalability concerns preventing its utilization in large scale manufacturing setups. For this reason, the research is more and more focused on the implementation of anion exchange chromatography (AEX), which exploits the slight difference in isoelectric point (pI) between the product (*i.e.* pI = 5.9) and impurity (*i.e.* pI = 6.3) [21–23]. It has been shown that, together with the stationary phase, the mobile phase composition strongly affects the separation performance, with the salt used in the gradient elution playing a major role on empty/full separation. In this direction, Keller et al. reported a systematic high-throughput screening aimed at evaluating the adsorption and recovery of AAV serotypes 8 and 9 from different resins and salts [21]. The authors highlighted that pH 9.0 allowed to reduce the capsid flow-through compared to more acidic environments, while improving the AAV recovery. This finding is shared with other works on the topic and is becoming the standard in the literature [24,25]. The choice of the salt used for the elution, instead, is very much debated. On one side, the quaternary ammonium salt tetramethylammonium chloride (TMAC) is recognized as the one allowing the highest resolution, supposedly due to the competition with quaternary ligands, commonly used in AEX, for AAV binding [26–28]. At the same time, this molecule is highly toxic, which makes its use in large scale applications questionable. This led to the exploration of alternative electrolytes, including sodium chloride, sodium acetate, ammonium acetate and choline chloride, all leading to reduced resolution with respect to TMAC and variable separation outputs depending upon AAV serotype and stationary phase [15,29–31]. The choice of the adsorbent is indeed another subject of extensive investigation. Most of the stationary phases reported for preparative purposes are based on methacrylate resins functionalized with quaternary ammonium groups and with particle size from 30 to 50 μm [32–35]. Nonetheless, few examples exploiting monoliths can be found [22,36,37]. Regardless of the careful selection of mobile phase composition and stationary phase, the very similar chromatographic behavior of empty and full particles makes them largely co-elute in all the mentioned studies referred to single-column preparative processes. This introduces the phenomenon known in the literature as yield/purity tradeoff [38–40]. In order to achieve high purity, the collection window should be narrow enough to discard the impurities and the portion of the product co-eluting with them. This evidently penalizes the full particle recovery, or yield. At the opposite, to improve the latter, the collection window should be enlarged, which ultimately leads to include impurities in the product pool.

To alleviate this tradeoff, multicolumn countercurrent solvent gradient purification (MCSGP) was demonstrated a valuable solution. This process, reported in the literature for the polishing of monoclonal antibodies [41–43], peptides [44,45], proteins [46,47], and oligonucleotides [48–50], alternates two twin columns throughout parallel and interconnected stages. Briefly, in a first batch phase (B1), the columns are disconnected and the weakly adsorbed impurities (W) are discarded from the upstream column during a linear gradient, while the downstream column is regenerated. In the following stage, the two columns are interconnected (IC1) to internally recycle the product (P) co-eluting with W from the upstream column, which is continuing its linear gradient, to the downstream one. Then, in a second batch step (B2), P is collected from the former, while the latter is fed with fresh mixture. Finally, in a second interconnected phase (IC2), the impure fraction containing P and strongly adsorbed impurities (S) is internally recycled from the upstream to the downstream column. The interested reader can find more detailed descriptions of the process at [38,40,51]. The combination of these four steps represents a switch, which is repeated a second time with the two columns exchanged in position to complete a full cycle. The latter then comprises two product collections and two re-feedings, once per column. Because of the automated internal recycle of impure side-fractions, MCSGP can achieve high purity and yield simultaneously, thus overcoming a major limit in single-column chromatography. However, despite the potential of MCSGP, to the best of our knowledge, no applications to empty/full AAV separation are reported. This may be ascribed to the difficult process design and high costs of AAVs, which limit the possibilities for experimentation. At the same time, MCSGP could provide a decisive advantage over batch chromatography.

Therefore, the aim of this work is the establishment of an efficient MCSGP for the enrichment of full capsids guided by a mechanistic model to reduce the time and resources dedicated to process design. This would provide a viable process allowing to sustain the expected growth in therapies based on AAVs. In this direction, we developed a mechanistic model for the anion exchange chromatographic separation of empty and full AAV2 capsids. This was tackled as a binary separation, since impurities other than empty particles (*e.g.* partially filled and overfilled particles) are often minor and their reliable isolation and quantification is challenging. The model was calibrated from six linear gradient elution experiments performed at different gradient slopes and salt concentrations in the wash step. By leveraging this trained model, an *in silico* optimization strategy for the single-column process was proposed, with the aim of obtaining a robust set-point to be converted to MCSGP. The objective of this optimization was the maximization of yield and productivity at a set purity specification (Pspec). We demonstrated that these two parameters cannot be increased simultaneously, but the process parameters leading to an increase in yield were also associated to poor productivity and *vice versa*. The two most performing operations, leading to the maximum yield and productivity, respectively, were experimentally validated, allowing to conclude on the good accuracy of the model.

Finally, the model was exploited for the simulation of MCSGP, which required no further parameter tuning, m as demonstrated by comparing the model results with *ad hoc* experimental data on AAV concentration at different MCSGP times, measured by taking fractions from the two columns across the different phases. By converting the optimal batch configurations to MCSGP, we provided a region of operability for this process in terms of yield and productivity at fixed Pspec. Inside this region, the most convenient process was experimentally validated, which allowed to conclude on the possibility of simultaneously increasing the productivity and recovery of full capsids at the set Pspec, compared to the single-column operation. Thus, while most of the studies in the literature are focused on the exploration of different stationary phases and eluents to improve the performance in empty/full separations, we demonstrated in this work that MCSGP represents a valuable process for the large scale biomanufacturing of AAV-based gene therapies, and can be designed from a small set of experimental data by taking advantage of a relatively simple mechanistic model of the operation.

2. Materials and methods

2.1. Materials

Tris(hydroxymethyl)aminomethane (Tris, ≥99.8 %, MW=121.14 g/mol), magnesium chloride ($MgCl_2$, ≥98.0 %, anhydrous, MW=95.21 g/mol), tetramethylammonium chloride (TMAC, ≥98.0 %, MW=109.60 g/mol), sodium acetate (NaOAc, ≥99.0 %, MW=82.03 g/mol), hydrochloric acid (HCl, 36.5–38.0 %), sodium hydroxide (NaOH, ≥98.0 %, MW=40.00 g/mol), sodium chloride (NaCl, ≥98.0 %, MW=58.44 g/mol), Poloxamer 188 and HPLC-grade water were purchased from Merck and used as received.

The empty/full AAV mixture was manufactured on demand by Sirion Biotech and provided at a concentration of 1.00E13 viral particles (VP)/mL. The full AAVs contained a green fluorescent protein reporter gene

and a cytomegalovirus promoter. The production cell line is HEK293T and polyethyleneimine was used as transfection reagent. The virus harvest was performed 48 h after transfection by lysing the cells with a solution of 0.1 % triton. A primary AAV capture was performed with a Poros™ CaptureSelect™ AAV-X (ThermoFisher) and finally the viral particles were formulated in phosphate-buffered saline (PBS) + 0.014 % Tween™ 20 by dialysis using a Slide-A-Lyzer® dialysis cassette with a molecular weight cut-off of 10 kg/mol. Aliquots of 2 mL were stored at −80 °C until usage.

All the mobile phases reported in the following were buffered to pH = (9.0 ± 0.2) by drop-wise addition of a 5 M HCl solution and were filtered through 0.22 μm polyvinylidene fluoride membranes before usage.

2.2. AAV mixture and fraction analysis

The crude AAV mixture, the fractions collected during single-column linear gradient elutions as well as the product pools collected during each switch of MCSGP were analyzed by high performance liquid chromatography (HPLC) to quantify the empty and full particle concentration.

The analysis was performed at 30 °C on an Agilent 1200 chromatograph equipped with an Agilent Bio SAX NP5 column (4.6 × 50 mm, 5 μm particle size, nonporous particles). The equilibration buffer (buffer A) is a 70 mM Tris, 2 mM $MgCl_2$ solution. The elution buffer (buffer B) is as buffer A but with the addition of 800 mM TMAC. For each run, 100 μL of sample were injected through an autosampler equipped with a 100 μL injection loop.

The gradient conditions were adapted from the literature [52]. Specifically, the flowrate was constant to 0.35 mL/min, while the volume fraction of buffer B was increased from 0 to 12.5 % in 2 min, kept constant for 5 min, increased to 37.5 % in the following 20 min, brought to 90 % in 0.1 min and maintained for 3 min before being lowered back to 0 % to re-equilibrate the system for 15 min.

Double detection was performed using the fluorescence detector Agilent 1260 Infinity, with excitation at 280 nm and emission at 350 nm, and a diode array detector at both 254 and 280 nm.

A representative chromatogram for the AAV crude is shown in **Figure S1** (see Supporting Information). The purity in each sample was evaluated from the fluorescence signal as the ratio between the area under the peak of the full particles and the sum of the areas for empty and full AAVs. The absolute concentration of particles was measured by comparing the areas under the corresponding peaks in the chromatogram with a calibration curve obtained by injecting AAVs at known concentration.

2.3. Preparative single-column experiments

Batch empty/full separations were performed on a ContiChrom® CUBE 30 (YMC ChromaCon). This comprises an external BlueShadow 40D UV/Vis detector (Knauer), set at a wavelength of 260 nm, and a Foxy® R1 fraction collector (Teledyne Isco). An internal detector was used to track the conductivity as well as the absorbance at 280 nm of the solution at the column outlet. All the runs were performed at 25 °C, through an Azura® CT2.1 thermostat with solvent pre-heat cartridge (Knauer). A prepacked Fractogel® EMD TMAE (S) 1 mL minichrom column (0.8 × 2 cm, particle size 20–40 μm) from Merck Life Science was used for the separation.

The equilibration buffer (buffer A prep) comprised 70 mM Tris, 2 mM $MgCl_2$, and 1 % Poloxamer 188. The elution buffer (buffer B prep) is as buffer A prep but with the addition of 500 mM NaOAc as modifier.

The concentrated AAV feedstock at 1.00E13 VP/mL was diluted with buffer A prep to 5.00E11 VP/mL before loading to the system. Different combinations of gradient durations and boundaries, wash duration and volume fraction of buffer B prep during the equilibration and wash were tested to assess the impacts of these parameters on the performance of the separation. The specific conditions for preparative single-column experiments are summarized in Table 1.

During the gradient, fractions of the eluate from the column were collected, filled into glass vials without further treatment, and analyzed via HPLC as reported in Section 2.2. From each sample, the purity was measured as the ratio between the area under the peak of full particles and the sum of the areas of empty and full AAVs in the fluorescence signal. Yield (Y) and productivity (Prod) were determined for each fraction according to Eqs. (1)–(2).

$$Y_i\ [\%] = \frac{C_i^F V_i}{C_{feed}^F V_{feed}} * 100 \tag{1}$$

$$Prod_i\ \left[\frac{VP}{L_{resin} h}\right] = \frac{C_i^F V_i}{V_{col} t_{batch}} \tag{2}$$

where C_i^F and C_{feed}^F [VP/mL] are the full particle concentrations in the i^{th} fraction and in the feed, respectively, V_i [mL] is the volume of the fraction i, V_{feed} [mL] the volume of crude mixture injected into the system, V_{col} [L_{resin}] the volume of the column and t_{batch} [h] the process duration.

The Pareto fronts yield *vs.* purity were obtained by pooling together contiguous fractions to simulate different collection windows.

2.4. MCSGP

MCSGP was performed in twin-column mode using two Fractogel® EMD TMAE (S) 1 mL minichrom columns (0.8 × 2 cm each, particle size 20–40 μm) from Merck Life Science. The process was operated on a ContiChrom® CUBE 30 (YMC ChromaCon) equipped with two external BlueShadow 40D UV/Vis detectors set at 260 nm and two internal detectors recording the UV absorbance at 280 nm and the conductivity at the outlet of each column. The operation was performed at 25 °C set using an Azura® CT2.1 thermostat with a solvent pre-heat cartridge for each column (Knauer), using the same preparative buffers reported in Section 2.3.

The design of MCSGP was performed from a batch run, using the same amount of mixture fed to one of the two columns during the start-up and the same gradient slope. After the start-up, the volume of AAV

Table 1
Operating parameters adopted for the single-column empty/full AAV separation.

Parameter	Unit	Value
Equilibration Duration	[Column volumes (CV)]	5.0
Equilibration Flow Rate	[mL/min]	1.00
Buffer B Prep in Equilibration	[%]	From 23 to 50
Feed Concentration	[VP/mL]	5.00E11
Loaded Amount	[VP/mL_{resin}]	2.00E12
Loading Flow Rate	[mL/min]	0.50
Wash Duration	[Column volumes (CV)]	From 0.0 to 5.0
Wash Flow Rate	[mL/min]	0.50
Buffer B Prep in Wash	[%]	From 23 to 50
Gradient Duration	[Column volumes (CV)]	From 10.0 to 30.0
Gradient Flow Rate	[mL/min]	0.35
Gradient Boundaries	[%]	Start: From 40 to 50; Stop: From 70 to 80
Strip Duration	[Column volumes (CV)]	4.0
Strip Flow Rate	[mL/min]	1.00
Buffer B Prep in Strip	[%]	90
Re-Equilibration Duration	[Column volumes (CV)]	5.0
Re-Equilibration Flow Rate	[mL/min]	1.00
Buffer B Prep in *Re*-Equilibration	[%]	From 23 to 50

mixture fed during each switch was calculated in order to keep the mass of full particles in the system constant. Four characteristic times were selected to define the boundaries for each phase of MCSGP. The time t_1 set the start of the gradient and correspondingly of B1 and was chosen as the time at the start of the gradient in the corresponding design-batch process. The IC1 step is conducted between t_2 and t_3, with the former obtained after model-based design and the latter to reach the target Pspec. Finally, the second batch phase B2 is performed between t_3 and t_4, with the latter set at the end of the full particle elution. During the internal recycling of the impure empty/full fraction, an inline dilution (ID) using buffer A prep was applied to the eluate from the upstream column to restore binding conditions in the receiving one. In particular, the flow rate of ID was adjusted in order to reduce the modifier concentration in the stream to the value at the beginning of the gradient. Whenever an imposed maximum flow rate of 0.67 mL/min was overcome by the combination of recycled stream and dilution buffer, the former was reduced accordingly. In a typical run, the main operating parameters are summarized in Table 2 as an example.

The product pool was collected twice per cycle, once from each column, and analyzed via HPLC following the protocol reported in Section 2.2. From this analysis, the yield and productivity of the switch *i* (Y_i and $Prod_i$) were determined according to Eqs. (3)–(4), respectively.

$$Y_i\ [\%] = \frac{C_i^F V_i}{C_{feed}^F V_{Re-feed}} * 100 \tag{3}$$

$$Prod_i \left[\frac{VP}{L_{resin} h}\right] = \frac{C_i^F V_i}{2\ V_{col} t_{Switch}} \tag{4}$$

where C_i^F and C_{feed}^F [VP/mL] are the full particle concentrations in the product pool from switch *i* and in the crude mixture, respectively, V_i [mL] is the volume of the product pool collected during switch *i*, $V_{Re\text{-}feed}$ [mL] the volume of mixture injected into the system during every switch of the cyclic operation, V_{col} [L_{resin}] the volume of column and t_{Switch} [h] the duration of a single switch (*i.e.* $t_{Cycle}/2$).

2.5. Model equations

The transport of AAVs along the column was described through the equilibrium-dispersive model (Eq. (5)) [53].

$$\frac{\partial C_i}{\partial t} = -v\frac{\partial C_i}{\partial z} + D_{ax,i}\frac{\partial^2 C_i}{\partial z^2} - \frac{1-\varepsilon}{\varepsilon}\frac{\partial q_i}{\partial t} \tag{5}$$

where C_i [VP/mL] is the instantaneous liquid concentration of the species *i*, q_i [VP/mL_{resin}] the corresponding instantaneous average concentration in the solid, v [cm/min] is the interstitial velocity, z [cm] the longitudinal position along the column, $D_{ax,i}$ [cm^2/min] the axial dispersion coefficient for the species *i* and ε [-] the void fraction. These equations were solved considering the column clean and re-equilibrated to the desired salt concentration at $t = 0$ and using Danckwerts' type boundary conditions as reported in Eqs. (6)–(7).

$$vC_{i,feed} = vC_i(t, z=0) - D_{ax,i}\left.\frac{\partial C_i}{\partial z}\right|_{z=0} \tag{6}$$

$$\left.\frac{\partial C_i}{\partial z}\right|_{(z=L_C)} = 0 \tag{7}$$

The mass transfer inside the stationary phase was treated using the lumped rate model as reported in Eq. (8) [54–57].

$$\frac{\partial q_i}{\partial t} = k_{LDF,i}\left(q_i^* - q_i\right) \tag{8}$$

where $k_{LDF,i}$ [min^{-1}] is the lumped rate constant, which is assumed to be equal for empty and full AAVs, given their very similar size and surface composition, and q_i^* [VP/mL_{resin}] is the concentration of species *i* in the solid phase at thermodynamic equilibrium with the liquid phase. The latter was described through the Langmuir isotherm in the form shown in Eq. (9), considering parameters dependent on the local buffer B vol. % (%B) through the linear solvent strength model [58–60].

$$q_i^* = \frac{H_i C_i}{1 + \sum_{j=1}^{N=2}\frac{H_j}{q_{sat}} C_j} = \frac{H_{0,i}\exp\left(-S_{H,i}\%B\right)C_i}{1 + \sum_{j=1}^{N=2}\frac{H_{0,j}}{q_{sat,0}}\exp\left[-\left(S_{H,j} - S_{q_{sat}}\right)\%B\right]C_j} \tag{9}$$

where N is the number of components (2 in this case, *i.e.* empty and full AAVs), H_i [mL/mL_{resin}] is the Henry constant for the component *i*, $H_{0,i}$ [mL/mL_{resin}] and $S_{H,i}$ [-] its corresponding pre-exponential factor and sensitivity to the modifier, q_{sat} [VP/mL_{resin}] is the saturation capacity for the resin, with its pre-exponential factor $q_{sat,0}$ [VP/mL_{resin}] and sensitivity S_{qsat} [-], considered equal for full and empty particles.

The same model was used also for the description of the mass transport of modifier in the column. However, in this case we assumed no adsorption, which is translated in $q^*_{modifier} = 0$ and $\frac{\partial q_{modifier}}{\partial t} = 0$. The concentration of modifier was then converted to conductivity by applying the Kohlrausch's law [53,61].

In the same way, the different dead volumes included in the equipment (*i.e.* capillaries, selection valves and detector flow cells) were treated as plug flow systems and described through the same Eqs. (5)–(7) considering liquid phase only ($\frac{\partial q_i}{\partial t} = 0$) and $\varepsilon = 1$.

The partial differential equations in space and time were reduced to a system of ordinary differential equations (ODEs) by discretization of the spatial coordinate using the finite difference method [53]. The discretized forms of Eqs. (5)–(9) are reported in the Supporting Information (see **Eqs. S1-S5**). This system of ODEs was numerically solved using the *ode15s* routine in MATLAB.

The model parameters $k_{LDF,i}$, $D_{ax,i}$, $H_{0,i}$, $S_{H,i}$, $q_{sat,0}$ and S_{qsat} were estimated by nonlinear regression of six gradient elution experiments from which at least 12 fractions each were collected and analyzed via HPLC. The objective function F for data fitting is reported in Eq. (10).

$$F = \sum_{j=1}^{Nexp} \times \sum_{i=1}^{N=2}\left[\frac{\left(\mu_{i,j}^{exp} - \mu_{i,j}^{mod}\right)^2}{\left(\mu_{i,j}^{exp}\right)^2} + \frac{\left(\sigma^{2\,exp}_{i,j} - \sigma^{2\,mod}_{i,j}\right)^2}{\left(\sigma^{2\,exp}_{i,j}\right)^2} + \frac{\left(HETP_{i,j}^{exp} - HETP_{i,j}^{mod}\right)^2}{\left(HETP_{i,j}^{exp}\right)^2}\right] \tag{10}$$

where μ [min] is the average retention time, σ^2 [min^2] the peak variance, and HETP [cm] the height equivalent to a theoretical plate. These parameters were evaluated for empty and full particles both from the modelled chromatogram and experimental peaks as summarized in Eqs.

Table 2
Exemplary operating parameters for MCSGP.

Parameter	Units	Value
Loaded Amount in Start-Up	[VP/mL_{resin}]	2.00E12
Loaded Amount per Switch	[VP/mL_{resin}]	7.50E11
Loading Flow Rate	[mL/min]	0.35
Gradient Duration	[Column volumes (CV)]	30.0
Gradient Flow Rate	[mL/min]	0.35
Buffer B prep at t_1	[%]	48.0
Buffer B Prep at t_2	[%]	59.0
Buffer B Prep at t_3	[%]	62.4
Buffer B Prep at t_4	[%]	66.7
Dilution Flow Rate	[mL/min]	0.11
Strip Duration	[Column volumes (CV)]	4.0
Strip Flow Rate	[mL/min]	1.00
Buffer B Prep in Strip	[%]	90
Re-Equilibration Duration	[Column volumes (CV)]	10.0
Re-Equilibration Flow Rate	[mL/min]	1.00
Buffer B Prep in *Re*-Equilibration	[%]	23
Cycle Duration	[min]	147

(11)–(13).

$$\mu_i = \frac{\int_0^\infty C_i\ t\ dt}{\int_0^\infty C_i\ dt} \tag{11}$$

$$\sigma_i^2 = \frac{\int_0^\infty C_i\ (t-\mu_i)^2\ dt}{\int_0^\infty C_i\ dt} \tag{12}$$

$$HETP_i = L_{col}\frac{\sigma_i^2}{\mu_i^2} \tag{13}$$

The minimization problem was solved with the *ga* routine coupled with the hybrid function *fmincon* in MATLAB. A total of 50 generations were run, each one comprising 400 individuals. The 95 % confidence interval was estimated based on the analysis of the Jacobian matrix and asymptotic normal distribution for the parameter estimate. This is done using the routine *nlparci* in MATLAB, returning the 95 % confidence intervals for nonlinear least-squares parameter estimates.

2.6. Batch optimization

The established model for empty/full separations was exploited for an *in silico* optimization of the process. Specifically, we considered four variables, namely the gradient and wash durations, salt concentration in the wash step (considered equal to the equilibration concentration) and salt concentration at the gradient start. In particular, the gradient duration was allowed to vary in the range [5,30] CV, the wash duration in the interval [0, 15] CV, the salt concentration in the wash in the range [0, 250] mM and the modifier molarity at the start of the gradient in the interval [50, 300] mM. The latter was also constrained to be larger or equal to the salt concentration in the wash. All the remaining process parameters were fixed and as reported in Table 1. As performance indicators, we considered the yield and productivity at a fixed minimum acceptable purity (Pspec). The optimization problem was solved for four different values of Pspec, *i.e.* 60.0 %, 65.0 %, 70.0 % and 75.0 %, using the *gamultiobj* routine in MATLAB with 50 generations and 400 individuals. In particular, for each combination of process variables, the corresponding chromatogram was generated. For the evaluation of the performance indicators, the definition of a collection window is required. For this, the end of product collection (t_{End}) was considered as the time where $C_{Full} < 10^{-3}$ VP/mL. The time for starting the product collection (t_{Start}) was initially set equal to t_{End} and progressively anticipated until the purity measured for that specific collection window was larger than Pspec. After having defined the characteristic times for product collection, the yield and productivity were computed according to Eqs. (14)–(15).

$$Y[\%] = \frac{Q_{elution}\int_{t_{Start}}^{t_{End}} C_{Full}\ dt}{Q_{load}C_{Full,feed}t_{load}} * 100 \tag{14}$$

$$Prod\left[\frac{VP}{L_{resin}h}\right] = \frac{Q_{elution}\int_{t_{Start}}^{t_{End}} C_{Full}\ dt}{V_{col}t_{Batch}} \tag{15}$$

where $Q_{elution}$ and Q_{load} [mL/min] are the volumetric flow rates used during elution and loading, respectively, t_{load} [min] is the loading duration, t_{Batch} [h] is the total process duration, and V_{col} [L_{resin}] is the column volume.

This optimization led to a tradeoff between yield and productivity at any Pspec, mainly driven by the duration of the gradient and wash steps. The two processes maximizing either the productivity or the yield at Pspec=70.0 % were run experimentally using the equipment and procedures reported in Section 2.3. These experiments were also considered for model validation, as the specific operating conditions were different from those used for parameter estimation.

3. Results and discussion

3.1. Single-column empty/full separation

In this work, we investigated the anion exchange chromatographic separation of AAVs serotype 2. The crude mixture containing empty and full particles was first analyzed via HPLC according to the protocol reported in Section 2.2. The analytical chromatogram, recorded through both a fluorescence and a diode array detector at 254 and 280 nm, is shown in **Figure S1** (see Supporting Information). The fluorescence signal highlights two major peaks, with a difference in the retention time of 2.40 min and a chromatographic resolution of 0.95. The early-eluting peak was attributed to the empty AAVs, due to their higher pI compared to the full AAVs, eluting later. This attribution is supported by the ratio of the areas under the UV signals at 254 and 280 nm. For the first peak, this ratio is equal to 0.63, in line with previous observations demonstrating a ratio of 0.6 for purely empty capsids. On the other side, the same ratio for the second peak is equal to 1.32, in good agreement with the previous findings reporting a ratio of 1.3 for full particles enveloping a single-stranded DNA with a length of 4700 base pairs [27,62]. By integration of the fluorescence signal, the purity of full particles in this crude mixture was 18.3 %, clearly indicating the necessity of an enrichment to improve the clinical relevance of these gene therapy products.

To tackle this, we started from a systematic analysis of the role of the gradient duration and salt concentration in the wash step on the performance of a single-column chromatographic operation. A total of six linear gradient elutions were performed and, for each experiment, different fractions were collected and analyzed via HPLC to determine the respective concentration in empty and full particles. **Figure S2** shows the preparative chromatograms at the different operating conditions tested. As anticipated, due to the very similar physicochemical properties of empty and full AAVs, a baseline separation could never be accomplished when using a resin with particle size typical for preparative chromatography (in our case Fractogel® EMD TMAE (S), 20–40 µm). Conversely, the peaks for the two species are partially overlapped, which introduces a tradeoff between yield and purity. In fact, when selecting a narrow collection window, a pool with high content in full AAVs could be obtained, but at reduced product recovery. The opposite was achieved instead when selecting a broad collection window. This tradeoff is reflected in the Pareto fronts reported for the different experiments in Fig. 1 and **Table S1**, where the yield and purity were calculated for different hypothetical collection windows by considering the aggregation of adjacent fractions from the purest to the richest in empty capsids. The yield and purity associated to each fraction were evaluated after HPLC analysis according to Eq. (1) and as the ratio between the area of full particles and total area, respectively.

By comparing the results at different gradient lengths (Fig. 1a), it is possible to observe that an increase in this parameter led to higher chromatographic resolution, allowing higher and higher full purities to be accessed. At the same time, this had also an impact on the overall particle yield, represented by the point on the far most right of the Pareto front. This value increased for shallower gradients, allowing to recover overall more and more full particles. The explanation can be found in the high tendency of these AAVs to aggregate, which represents a critical source of mass loss in a chromatographic separation [63–65]. It may be concluded that a too fast increase in the solution conductivity may trigger this aggregation. Indeed, a similar trend was observed when investigating different percentages of buffer B Prep in the wash step (Fig. 1b). Here, it is possible to observe that the maximum yield in full particles drops with the salt concentration. When using 50 %vol. buffer B Prep in the wash step, <60 % of the loaded full particles could be recovered. The yield significantly improved at 40 and 42 %vol. buffer B Prep, with the latter leading also to the best purity. This highlights that an isocratic hold at intermediate salt concentrations is important to favor the empty/full separation for these AAV2.

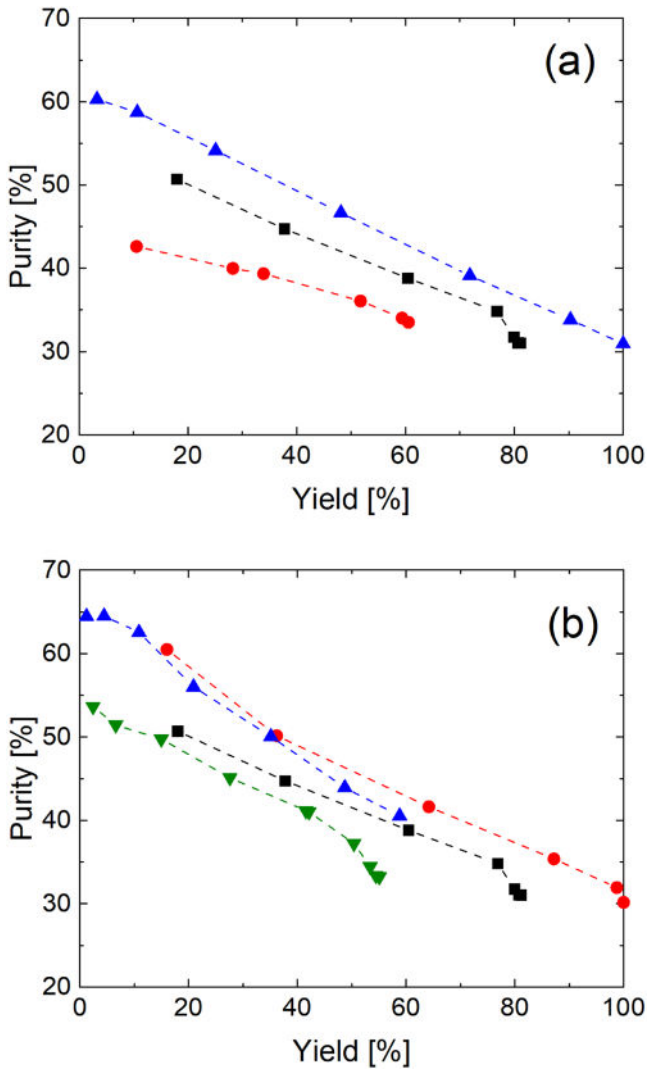

Fig. 1. (a) Pareto fronts yield *vs.* purity at different gradient lengths: 12 CV (●), 15 CV (■) and 25 CV (▲). (b) Pareto fronts yield *vs.* purity at different vol. % of buffer B prep in the wash step: 40 % (■), 42 % (●), 45 % (▲) and 50 % (▼). Yield is referred to the amount of full particles recovered out of the injected ones, while purity is the fraction of full particles over the total number of capsids, *i.e.* full + empty. Lines were added to facilitate the reading of the figure.

The experiments performed at different gradient duration and salt concentration in the wash step were exploited to train a mechanistic model of the anion exchange purification of this empty/full mixture. In particular, the isotherm parameters in Eq. (9), the axial dispersion coefficient (D_{ax}) and the linear driving force constant (k_{LDF}) for empty and full particles were regressed from the experimental results by minimizing the relative squared errors between the mean retention time (μ), peak variance (σ^2) and HETP (see Eq. (10)). The set of parameters leading to the best fitting with the 95 % confidence interval are reported in **Table S2**, while the comparison between model and experimental results is shown in **Figure S2**. By looking at the values obtained from the regression, it is possible to observe that the only difference between empty and full particles lies in the pre-exponential factor for the Henry coefficient (H_0), which is slightly higher for the latter, as expected by its smaller pI and hence larger affinity towards anion exchangers. This supports the consistency of the parameters obtained. On the other side, the sensitivity for the modifier S_H is the same for the two species. This explains the difficulty in this separation, as the behavior for the two components in elution chromatography is indeed very similar. With this combination of parameters, the model is able to accurately reproduce the elution behavior, catching the mean retention time as well as the peak height, in most of the conditions. The agreement is good also in those situations, like in **Figure S2a, b** and **d**, where the full particles end up eluting in the strip phase. The higher velocity in this step causes a steep tail of the peak, which is properly captured by the model.

It is worth highlighting that, despite a Langmuir isotherm was considered herein for sake of generality, the resin is not saturated at the concentrations tested in this work. Indeed, in **Figure S3**, we compared the elution profile predicted by the model considering Langmuir adsorption with that obtained in the case of a linear isotherm with the same Henry coefficient parameters (H_0 and S_H) regressed from the experimental data. Only a minimal anticipation can be observed in the elution of empty particles when considering a Langmuir model, due to the limited competition with full AAVs. Therefore, in this specific case, a linear isotherm can be adopted as well, reaching similar results.

Given the good accuracy of the model in reproducing the experimental observations, this was exploited for an *in silico* optimization of the single-column process. In particular, different durations of the wash (from 0 to 5 CV) and of the gradient (from 5 to 30 CV) as well as different salt concentrations in the wash (from 0 to 250 mM) and at the gradient start (from 0 to 300 mM) were explored. For each tested combination of these operating parameters, a collection window was selected in order to reach a selected Pspec and the yield and productivity of the process were determined and used as optimization functions. This operation was repeated for 4 different values of Pspec, *i.e.* 60.0, 65.0, 70.0 and 75.0 %. In all the situations, a tradeoff between yield and productivity mainly driven by the gradient duration was observed. This behavior is reflected in the Pareto fronts shown in Fig. 2a. These curves represent the maximum achievable productivity at any value of yield for a given Pspec. In other words, all the points below these fronts are potentially accessible, while in no conditions, at least in the range of operating parameters investigated, a larger productivity can be obtained. In this sense, all the points on the front are optimal. However, for a single-column operation, it is not possible to maximize both yield and productivity simultaneously, which is a major drawback of batch chromatography.

If we focus on a single Pareto front, for example the one obtained at 70.0 % purity, the point at maximum productivity and minimum yield was achieved with short wash (*i.e.* 3 CV) and gradient (*i.e.* 20 CV). With these operating parameters, the resolution between empty and full AAVs is rather limited, which explains why only 11.1 % of loaded full particles could be recovered at the required Pspec. On the other side, given the short duration of the process, the productivity was 3.73E13 VP/(L_{resin} h). The dual situation is achieved with long wash (*i.e.* 4.6 CV), and, even more importantly, long gradient (*i.e.* 30 CV). This condition led to a higher resolution, and hence 12.3 % of the loaded full particles could be collected while satisfying the Pspec. However, the longer process reduced the productivity to 3.49E13 VP/(L h). Then, in order to select the best process, one should first define its target performance. On the other side, the salt concentration in the wash step and at the gradient start were invariably obtained in a limited range, namely 85 – 125 mM and 235 – 260 mM, respectively, playing a minor role on this observed tradeoff.

If Pspec is changed, this tradeoff between yield and productivity is preserved. However, for higher Pspec, the Pareto fronts are shifted towards lower and lower yield and productivity, given the narrower collection windows required to satisfy more and more stringent purity constraints as well as the longer duration of the gradient required to reach such high purity. On the other side, a less severe Pspec allowed improved yield and productivity to be achieved.

From these *in silico* Pareto fronts, we considered the operating conditions leading to the maximum productivity and those leading to the maximum yield at Pspec = 70.0 % and reproduced them experimentally. These optimal process conditions are summarized in Table 3. The experimental chromatograms are shown in Fig. 2b,c (symbols) and the

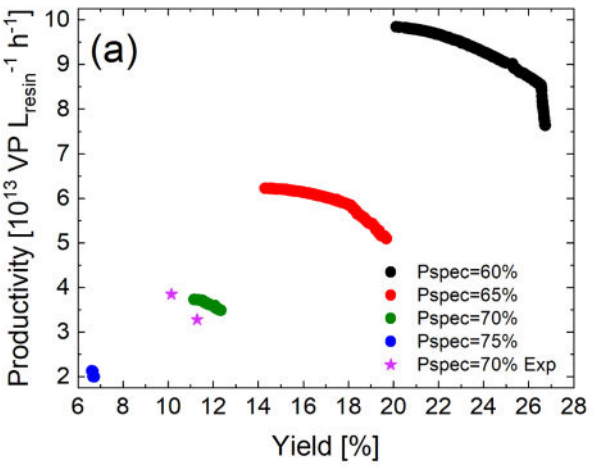

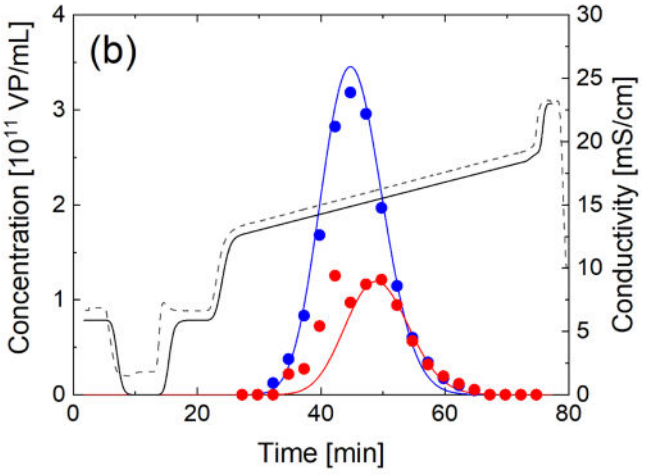

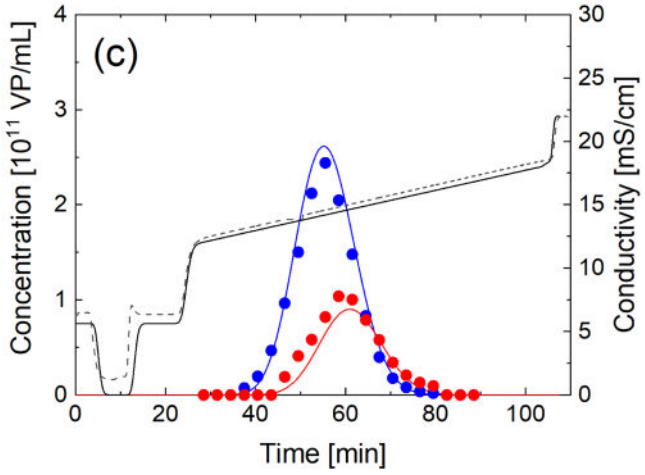

Fig. 2. (a) Pareto fronts yield *vs.* productivity at fixed Pspec and comparison with the experimental validation of the processes leading to the maximum yield and productivity at Pspec = 70.0 % (magenta stars). (b) Preparative chromatogram of the process characterized by the maximum productivity and (c) for the process with the maximum yield. Continuous lines: model predictions for conductivity (black), empty (blue) and full (red) particle concentrations. Dots: experimental concentrations for empty (blue) and full (red) particles. Dashed line: experimental measurement of conductivity.

Table 3
Operating parameters maximizing either the yield or the productivity at Pspec = 70.0 %.

Operating Parameter	Unit	Process with Max Productivity	Process with Max Yield
Purity Specification	[%]	70.0	70.0
Wash Duration	[CV]	3	4.6
Gradient Duration	[CV]	20	30
Salt Concentration in Wash	[mM]	110	115
Salt Concentration at Gradient Start	[mM]	250	240
Yield Model	[%]	11.1	12.3
Yield Experiment	[%]	10.2	11.3
Productivity Model	[VP L_{resin}^{-1} h^{-1}]	3.73E13	3.49E13
Productivity Experiment	[VP L_{resin}^{-1} h^{-1}]	3.85E13	3.28E13

raw data in terms of concentration of empty and full particles during time, as measured after HPLC analysis of fractions taken during the gradient after calibration with standards at known concentration, are reported in **Table S3**. It is possible to observe that the model predictions (lines in Fig. 2b,c) are in good agreement with the experimental results. This provides a reliable way for validating the mechanistic model developed in this work, as the conditions tested are significantly different from those used for training. At the same time, the good agreement between model and experiments led to similar performance indicators (evaluated, in the case of the experimental tests according to Eqs. (1)-(2)). Indeed, by looking at Fig. 2a, the experimental points (magenta stars) are very close to the extremes of the corresponding Pareto front determined *in silico*. This testifies the relevance of a model-based optimization, essential to define optimal operating conditions while reducing the effort and the material required for experimentation, which is particularly relevant in this case considering the high costs of these AAVs.

3.2. MCSGP for empty/full separation

Despite the optimal operating conditions identified through the *in silico* optimization procedure reported in this work, a single-column operation is invariably bound to a productivity/yield tradeoff, and can deliver only a very limited product recovery when a Pspec is set, as a result of a remarkable overlap between the empty and full peaks. With the aim of alleviating this tradeoff and recover more full particles in specification, we explored the implementation of MCSGP in its twin column version.

First, we wanted to verify the possibility of extending the chromatographic model developed for the batch process to MCSGP and its reliability. For this, we run the MCSGP of AAVs with the same gradient conditions and product collection window (from 61.6 min to 74.7 min) as the batch leading to the maximum yield (Table 3 and Fig. 2c), but recycling the portion of the chromatogram from 51.3 min to 61.6 min from one column to the other. To ensure this fraction was properly adsorbed in the receiving column, it was diluted in-line to restore the modifier concentration at the beginning of the gradient. The predicted chromatogram over 5 cycles and the corresponding conductivity signal measured experimentally are shown in **Figure S4**. By analyzing the predicted and measured conductivity, it is possible to conclude that the model properly catches the transport of modifier in the twin-column system, as well as the periodicity of the operation. On the other hand, the very low intensity of the UV signal for these AAVs prevented a fair comparison between the predicted and experimental chromatograms. Therefore, to further support the model reliability, the experiment was repeated this time fractionating the eluate from the first column during the discard of the empty capsids (B1 phase) as well as during the product collection (B2 phase). Similarly, fractionation of the recycled stream

(IC1 step) was performed at the inlet of the receiving column. The AAV concentration in these fractions, measured via HPLC, was compared with the model predictions in **Figure S5**. This comparison revealed a good agreement between the model and the experimental results, especially for the B1 and IC1 phases. This is a remarkable result, considering that no additional calibration was necessary to transfer the model from batch chromatography to MCSGP, expanding its scope to the model-based design of this twin column operation.

Indeed, we took advantage of this mechanistic model to transfer each operating condition leading to a point on the Pareto front with Pspec = 70.0 % in Fig. 2a to MCSGP. This was simulated for 10 cycles, keeping the same gradient conditions and collection window as the corresponding batch operation, but starting the recycle phase when the concentration of full particles reached 5 % of the predicted concentration at peak maximum. What we found out was that the amount of empty capsids removed from the system during the two batch phases (B1 and B2) was invariably lower than that re-fed in each switch, being the empty AAVs dominant in the crude mixture. This led to an accumulation of these impurities, which reduced the product pool purity switch after switch, as visible in **Fig. S6** for the process replicating the gradient conditions of the single-column experiment with the maximum yield (*i.e.* 30 CV gradient from 240 to 380 mM sodium acetate).

To circumvent this issue, we repeated the same analysis but this time starting the internal recycle at a characteristic time such that the amount of reintroduced empty capsids was lower than that removed during the B1 and B2 phases. As visible in Fig. 3a for the same process analyzed before, although this strategy enabled to discard a significant amount of empty capsids in the B1 step, it required the sacrifice of a fraction of full AAVs in the same phase. Indeed, this early discard of full capsids burdened the yield of the separation, which could not be higher than 72.0 %, as visible in Fig. 3b (the raw data are reported in **Table S4**). At the same time, this choice was rewarded with a process reaching already after 3 switches the steady state and ensuring consistent purity, yield and productivity.

By leveraging this design strategy, all the points on the yield-productivity Pareto front obtained for single-column separations at Pspec=70.0 % (see green dots in Fig. 2a) were converted to MCSGP and simulated for 10 cycles. For those process conditions allowing to respect the Pspec and to reach the steady state, the performance in terms of yield and productivity are displayed in Fig. 3c and compared with the corresponding design batches. This defines a sort of design space for MCSGP, or in other words the operability region for this periodically continuous process. It is possible to observe that MCSGP invariably leads to significantly higher yields and productivities compared to the single-

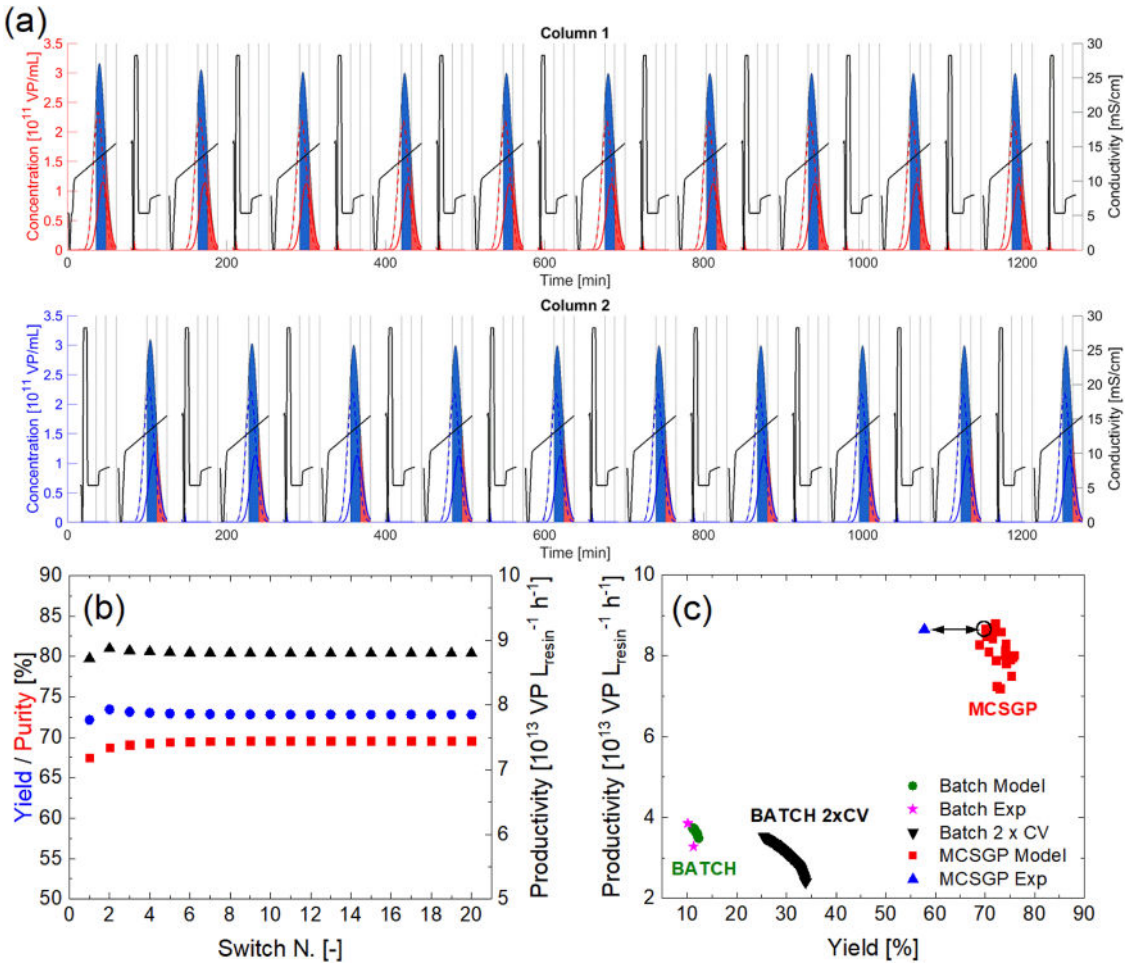

Fig. 3. (a) Chromatograms of the simulated MCSGP with 30 CV gradient from 240 to 380 mM sodium acetate. The black line represents the conductivity, the red lines the concentration for full (solid line) and empty (dashed line) AAVs eluting from column 1, while the blue lines the concentration for full (solid line) and empty (dashed line) AAVs eluting from column 2. The blue area highlights the portion of the chromatogram recycled from one column to the other, while the red area the product collection window. These areas are drawn below the total concentration in empty and full capsids. (b) Purity (■), yield (●) and productivity (▲) at each switch of the simulated MCSGP. (c) Comparison of batch with 1 × 1 mL column (●), batch with 2 × 1 mL column in series (▼), and MCSGP (■) performance in the separation of empty and full AAVs according to the optimized protocols with Pspec = 70.0 % as predicted by the model. The experimental validations are also reported for the batch with 1 × 1 mL column (★) and for MCSGP (▲). The latter was obtained by implementing the process conditions simulated in silico corresponding to the circled symbol in the plot.

column process. In addition, the tradeoff clearly visible for the latter could be alleviated when moving to the twin-column separation, which allowed to obtain simultaneously high yield and productivity while respecting Pspec. However, it is worth reminding that MCSGP involved 2 × 1 mL columns. Therefore, to make the comparison with the single-column operation fair, the latter was simulated considering 2 × 1 mL columns in series, the same amount of AAVs used in the startup of MCSGP and the same duration of wash, gradient and strip in terms of CVs (see black triangles in Fig. 3c). Given the double bed length, the separation was improved in this case and, at the same Pspec = 70.0 %, yields up to 35 % could be obtained. Still, these are significantly smaller than those accessed by MCSGP using the same resin volume, as a result of a more efficient management of the two columns. On the other hand, given that the resin volume was doubled and the overall process was longer on a time basis, the productivity of the batch with 2 × 1 mL columns was smaller even than that achieved with one single column, thus further highlighting the advantages of MCSGP.

Given the great potential of MCSGP, the process characterized by a 30 CV gradient from 240 to 380 mM sodium acetate was implemented experimentally for 4 cycles, by recycling the empty/full impure fraction from 52.8 to 63.5 min, while collecting the full capsids from 63.5 min to 71.6 min. The experimental chromatogram is shown in **Figure S7**, where the elution peaks from the two columns can be noticed, although with a poor intensity and significant noise, due to the low UV absorptivity of these particles. The product pools collected during the different switches were analyzed by HPLC and the concentration in full and empty capsids as well as the purity, yield and productivity as evaluated by Eqs. (3)-(4) are reported in **Table S5**. From this analysis, the performance reached at steady state (average of switches 6 to 8) were compared to those obtained for the corresponding single-column (1 × 1 mL column) separation in Fig. 3c and in Table 4. By looking at the figure, it is possible to observe that the experimental point is indeed very close to the productivity predicted by the model, confirming the reliability of the model-based design. On the other side, the yield was below the expectations, possibly due to difficulties in handling these particles following their poor colloidal stability. Also, at steady-state, MCSGP ensured a higher purity compared to the corresponding single-column operation as well as much larger yield = 57.8 % and productivity = 8.65E13 VP L_{resin}^{-1} h^{-1}, marking an improvement by 5.1 and 2.6 times, respectively.

This improved performance for the twin-column operation is also reflected into a more sustainable process. Indeed, for the single full capsid produced, as detailed in Table 4, MCSGP required less resin and consumed less water and salts. By assuming the resin with a density of 1 g/mL_{resin}, the different contributions were summed up to compute the process mass intensity (PMI), expressed as the amount of raw materials used to produce the single full capsid. While in the case of batch chromatography the PMI was 9.20E-10 g/VP, MCSGP could cut this number by a factor 3. This proves the potential of this technology not only in improving the performance for difficult center-cut purifications, but also in improving their sustainability, allowing for a more responsible management of resources.

Table 4
Comparison between batch and MCSGP in the empty/full separation in terms of process performance and process mass intensity (PMI). The PMI is calculated by summing up the contributions from the resin (assumed with density = 1 g/mL_{resin}), water, sodium acetate, Tris and Poloxamer 188.

Parameter	Unit	Batch	MCSGP	MCSGP Gain
Purity	[%]	69.8	75.6	+8.3 %
Yield	[%]	11.3	57.8	+411 %
Productivity	[VP L_{resin}^{-1} h^{-1}]	3.28E13	8.65E13	+164 %
Process Mass Intensity				
Resin	[mL_{resin}/VP]	1.64E-11	5.08E-12	−68.93 %
Water	[g/VP]	8.72E-10	2.93E-10	−66.42 %
Sodium acetate	[g/VP]	1.59E-11	4.62E-12	−70.94 %
Tris	[g/VP]	8.72E-12	2.93E-12	−66.42 %
Poloxamer 188	[g/VP]	7.39E-12	2.48E-12	−66.42 %
PMI	[g/VP]	9.20E-10	3.08E-10	−66.54 %

4. Conclusions

The separation of empty and full AAV capsids is still a major challenge limiting the outreach of this new therapeutic modality. This is hampered by very similar physicochemical properties between the two entities. Indeed, from 6 linear gradient elutions performed at different salt concentrations in the wash phase and gradient slopes, we developed a mechanistic model of their anion exchange separation. From this, we observed only a slight difference in the value of the pre-exponential coefficient of the Henry constant (H_0 = (3.34 ± 0.46)E5 for empty particles and H_0 = (4.93 ± 0.54)E5 for full AAVs), while their sensitivity to the modifier concentration was practically the same (S_H = 0.180 ± 0.003). This is responsible for an extended overlap of the corresponding chromatographic peaks in any tested condition. A model-based optimization strategy was developed for the single-column chromatographic separation, which revealed a tradeoff between productivity and yield when a constraint is placed on the minimum acceptable purity, as a result of this peak overlap. Considering the optimal configurations at Pspec=70 %, by increasing the duration of the gradient from 20 to 30 CV, higher resolutions can be achieved, thus increasing the amount of recoverable product from 10.2 to 11.3 %. On the other side, the productivity decreased from 3.73E13 to 3.49E13 VP/(L_{resin} h). This means that batch operations cannot reach simultaneously high yield and productivity. To overcome this limitation, we applied the calibrated model to the design of MCSGP, allowing fast and resource-effective process development. Under the condition of removing from the system an amount of empty capsids at least equal to that introduced by the refeeding step, a steady-state operation could be reached and maintained for at least 10 cycles. By simulating different process conditions, MCSGP invariably allowed to achieve much larger yields (>65 %) and productivities (>7.00E13 VP/(L_{resin} h)) compared to the single-column operations. This was validated experimentally, where MCSGP allowed to reach 75.6 % purity, 57.8 % yield in full particles and a productivity of 8.65E13 VP/(L_{resin} h). Comparing this performance to its batch counterpart, at comparable purity, the yield and productivity for the empty/full separation were improved by a factor 5.1 and 2.6, respectively. Additionally, the comparison of the process mass intensity between these two processes revealed a cut by a factor 3 of all the rubrics involved in the analysis, including resin, water and salts required for the single full capsid manufactured. We therefore demonstrated that the model-based design of MCSGP can extremely reduce the time and material consumed during process development, leading to an operation with great potential for bringing AAVs to maturity.

Abbreviations and Acronyms

AAVs	Adeno-associated viruses
AEX	Anion exchange chromatography
B	Batch
C_i	Concentration in the liquid phase for the i^{th} specie
CV	Column volume
D_{ax}	Axial dispersion coefficient
DNA	Deoxyribonucleic acid
$H_{0,i}$	Henry coefficient at 0 %B for the i^{th} specie
HEK	Human embryonic kidney
HETP	Hight equivalent to a theoretical plate
H_i	Henry coefficient for the i^{th} specie
HPLC	High performance liquid chromatography
IC	Interconnected
ID	Inline dilution
k_{LDF}	Linear driving force rate constant
L_{resin}	Liter of resin
MCSGP	Multicolumn countercurrent solvent gradient purification
NaOAc	Sodium acetate

(*continued on next page*)

(*continued*)

P	Product
PBS	Phosphate-buffered saline
pI	Isoelectric point
PMI	Process mass intensity
Prod	Productivity
Pspec	Purity specification
q_i	Average concentration in the solid phase for the i^{th} specie
q_i^*	Average concentration in the solid phase in equilibrium with the liquid one for the i^{th} specie
q_{sat}	Resin saturation capacity
$q_{sat,0}$	Resin saturation capacity at 0 %B
S	Strongly-adsorbed impurities
S_H	Sensitivity for the Henry coefficient from the modifier concentration
S_{qsat}	Sensitivity for the saturation capacity from the modifier concentration
t_{Cycle}	Cycle duration
TMAC	Tetramethylammonium chloride
Tris	Tris(hydroxyethyl)aminomethane
v	Interstitial velocity
VP	Viral particle
W	Weakly-adsorbed impurities
Y	Yield
ε	Interparticle void fraction
μ	Mean retention time calculated from the first-order moment of the distribution
σ^2	Peak variance

CRediT authorship contribution statement

Luca Ossi: Writing – review & editing, Validation, Investigation. **Helena Marie:** Writing – review & editing, Resources. **Michael Schulte:** Writing – review & editing, Supervision, Funding acquisition. **Mattia Sponchioni:** Writing – original draft, Software, Data curation, Conceptualization.

Declaration of competing interest

The authors declare that they have no known competing financial interests or personal relationships that could have appeared to influence the work reported in this paper.

Supplementary materials

Supplementary material associated with this article can be found, in the online version, at doi:10.1016/j.chroma.2025.466219.

Data availability

Data will be made available on request.

References

[1] S. Daya, K.I. Berns, Gene therapy using adeno-associated virus vectors, Clin. Microbiol. Rev. 21 (4) (2008) 583–593.
[2] A. Asokan, D.V. Schaffer, R.Jude Samulski, The AAV Vector toolkit: poised at the clinical crossroads, Mol. Therapy 20 (4) (2012) 699–708.
[3] C.W. Li, R.J. Samulski, Engineering adeno-associated virus vectors for gene therapy, Nature Rev. Genet. 21 (4) (2020) 255–272.
[4] X.D. Li, et al., Viral vector-based gene therapy, Int. J. Mol. Sci. 24 (9) (2023) 21.
[5] D. Wang, P.W.L. Tai, G.P. Gao, Adeno-associated virus vector as a platform for gene therapy delivery, Nature Rev. Drug Discov. 18 (5) (2019) 358–378.
[6] J.H. Wang, et al., Adeno-associated virus as a delivery vector for gene therapy of human diseases, Signal Transd. Targeted Therapy 9 (1) (2024) 33.
[7] M. Arjomandnejad, et al., Immunogenicity of recombinant adeno-associated virus (AAV) vectors for gene transfer, Biodrugs 37 (3) (2023) 311–329.
[8] C. Wetter, et al., Solution oligonucleotide APIs: regulatory considerations, Ther. Innov. Regul. Sci. 56 (3) (2022) 386–393.
[9] F. Mingozzi, K.A. High, Therapeutic in vivo gene transfer for genetic disease using AAV: progress and challenges, Nature Rev. Genetics 12 (5) (2011) 341–355.
[10] F. Meierrieks, et al., A novel and simplified anion exchange flow-through polishing approach for the separation of full from empty adeno-associated virus capsids, Biotechnol J 19 (10) (2024) e202400430.
[11] M.A. Robert, et al., Manufacturing of recombinant adeno-associated viruses using mammalian expression platforms, Biotechnol. J. 12 (3) (2017) 16.
[12] E.V. Tan, et al., HEK293 Cell line as a platform to produce recombinant proteins and viral vectors, Front Bioeng. Biotechnol. 9 (2021) 9.
[13] G. Ronzitti, D.-A. Gross, F. Mingozzi, Human immune responses to adeno-associated virus (AAV) vectors, Front Immunol. (2020) 11.
[14] K. Gao, et al., Empty virions in AAV8 vector preparations reduce transduction efficiency and may cause total viral particle dose-limiting side effects, Mol. Therapy - Methods Clin. Devel. 1 (2014) 9.
[15] S. Kurth, et al., Separation of full and empty adeno-associated virus capsids by anion-exchange chromatography using choline-type salts, Anal. Biochem. 686 (2024) 115421.
[16] Q. Weihong, et al., Scalable downstream strategies for purification of recombinant adeno- associated virus vectors in light of the properties, Curr. Pharm. Biotechnol. 16 (8) (2015) 684–695.
[17] B. Strobel, et al., Comparative analysis of cesium chloride- and iodixanol-based purification of recombinant adeno-associated viral vectors for preclinical applications, Hum Gene Ther. Methods 26 (4) (2015) 147–157.
[18] R. De-Luca, et al., Hybrid modeling of an ultracentrifugation process for separation of full and empty adeno-associated virus particles, Bioprocess Biosyst. Eng. 47 (6) (2024) 877–890.
[19] M. Wada, et al., Large-scale purification of functional AAV particles packaging the full genome using short-term ultracentrifugation with a zonal rotor, Gene Ther. (2023).
[20] Leigheb, S., et al., *Capture of adeno-associated viruses from clarified lysate by continuous flow ultracentrifugation: a comparative study of iodixanol and sucrose gradients.* J. Chem. Technol. Biotechnol.. **n/a**(n/a).
[21] W.R. Keller, et al., Rational downstream development for adeno-associated virus full/empty capsid separation – A streamlined methodology based on high-throughput screening and mechanistic modeling, J. Chromatogr. A 1716 (2024) 464632.
[22] D.P. Chen, et al., Tuning mobile phase properties to improve empty and full particle separation in adeno-associated virus productions by anion exchange chromatography, Biotechnol. J. 19 (1) (2024) 2300063.
[23] W.S. Kish, et al., Removal of empty capsids from high-dose adeno-associated virus 9 gene therapies, Biotechnol. Bioeng. 121 (8) (2024) 2500–2523.
[24] R.A. Lavoie, et al., Enrichment of adeno-associated virus serotype 5 full capsids by anion exchange chromatography with dual salt elution gradients, Biotechnol. Bioeng. 120 (10) (2023) 2953–2968.
[25] R. Rieser, et al., Comparison of different liquid chromatography-based purification strategies for adeno-associated virus vectors, Pharmaceutics 13 (5) (2021) 19.
[26] R. Rieser, et al., Comparison of different liquid chromatography-based purification strategies for adeno-associated virus vectors, Pharmaceutics 13 (5) (2021).
[27] K. Richter, et al., Purity and DNA content of AAV capsids assessed by analytical ultracentrifugation and orthogonal biophysical techniques, Eur. J. Pharmaceut. Biopharmaceut. 189 (2023) 68–83.
[28] Z. Wu, et al., Development of a two-dimensional liquid chromatography-mass spectrometry platform for simultaneous multi-attribute characterization of adeno-associated viruses, Anal. Chem. 94 (7) (2022) 3219–3226.
[29] P.R.H. Joshi, et al., Development of a scalable and robust AEX method for enriched rAAV preparations in genome-containing VCs of serotypes 5, 6, 8, and 9, Mol. Therapy - Methods Clinical Devel. 21 (2021) 341–356.
[30] S.L. Khatwani, A. Pavlova, Z. Pirot, Anion-exchange HPLC assay for separation and quantification of empty and full capsids in multiple adeno-associated virus serotypes, Mol. Therapy - Methods Clinical Devel. 21 (2021) 548–558.
[31] C. Wang, et al., Developing an Anion exchange chromatography assay for determining empty and full capsid contents in AAV6.2, Mol. Therapy - Methods Clin. Devel. 15 (2019) 257–263.
[32] M. Urabe, et al., Removal of empty capsids from type 1 adeno-associated virus vector stocks by anion-exchange chromatography potentiates transgene expression, Mol. Therapy 13 (4) (2006) 823–828.
[33] T. Tomono, et al., Ultracentrifugation-free chromatography-mediated large-scale purification of recombinant adeno-associated virus serotype 1 (rAAV1), Mol. Therapy - Methods Clin. Devel. 3 (2016) 15058.
[34] G. Qu, et al., Separation of adeno-associated virus type 2 empty particles from genome containing vectors by anion-exchange column chromatography, J. Virol. Methods 140 (1) (2007) 183–192.
[35] T. Tomono, et al., Highly efficient ultracentrifugation-free chromatographic purification of recombinant AAV serotype 9, Mol. Therapy - Methods Clin. Devel. 11 (2018) 180–190.
[36] M. Lock, M.R. Alvira, J.M. Wilson, Analysis of particle content of recombinant adeno-associated virus serotype 8 vectors by ion-exchange chromatography, Hum Gene Ther. Methods 23 (1) (2012) 56–64.
[37] J.P. Dickerson, et al., Allocation problems in ride-sharing platforms: online matching with offline reusable resources, ACM Trans. Econ. Comput. 9 (3) (2021) 13. Article.
[38] M. Catani, C. De Luca, Chapter three - application of Multicolumn countercurrent solvent gradient purification to the polishing of therapeutic proteins, in: D. Moscatelli, M. Sponchioni (Eds.), Advances in Chemical Engineering, Academic Press, 2022, pp. 69–100. Editors.
[39] M. Catani, et al., Oligonucleotides: current trends and innovative applications in the synthesis, characterization, and purification, Biotechnol. J. 15 (8) (2020) 1900226.
[40] H. Narayanan, M. Sponchioni, M. Morbidelli, Integration and digitalization in the manufacturing of therapeutic proteins, Chem. Eng. Sci. 248 (2022) 117159.

[41] S.-Y. Jing, et al., Improved process design for monoclonal antibody charge variants separation with multicolumn counter-current solvent gradient purification, J. Chromatogr. A 1707 (2023) 464292.
[42] T. Müller-Späth, et al., Chromatographic separation of three monoclonal antibody variants using multicolumn countercurrent solvent gradient purification (MCSGP), Biotechnol. Bioeng. 100 (6) (2008) 1166–1177.
[43] T. Müller-Späth, et al., Increasing the activity of monoclonal antibody therapeutics by continuous chromatography (MCSGP), Biotechnol. Bioeng. 107 (4) (2010) 652–662.
[44] C. De Luca, et al., Process intensification for the purification of peptidomimetics: the case of Icatibant through multicolumn countercurrent solvent gradient purification (MCSGP), Ind. Eng. Chem. Res. 60 (18) (2021) 6826–6834.
[45] C.D. Luca, et al., From batch to continuous chromatographic purification of a therapeutic peptide through multicolumn countercurrent solvent gradient purification, J. Chromatogr. A 1625 (2020).
[46] T.K. Kim, et al., Experimental design of the multicolumn Countercurrent Solvent gradient purification (MCSGP) unit for the separation of PEGylated proteins, Ind. Eng. Chem. Res. 60 (29) (2021) 10764–10776.
[47] T.K. Kim, et al., Design and economic investigation of a Multicolumn Countercurrent Solvent Gradient Purification unit for the separation of an industrially relevant PEGylated protein, J. Chromatogr. A 1681 (2022).
[48] I. Fioretti, et al., UV-based dynamic control improves the robustness of multicolumn countercurrent solvent gradient purification of oligonucleotides, Biotechnol. J. 19 (7) (2024) 2400170.
[49] I. Fioretti, et al., Continuous countercurrent chromatographic twin-column purification of oligonucleotides: the role of the displacement effect, Biotechnol. Bioeng. 119 (7) (2022) 1861–1872.
[50] R. Weldon, et al., Purification of a GalNAc-cluster-conjugated oligonucleotide by reversed-phase twin-column continuous chromatography, J. Chromatogr. A 1663 (2022) 462734.
[51] C. De Luca, et al., Modern trends in downstream processing of biotherapeutics through continuous chromatography: the potential of Multicolumn Countercurrent Solvent Gradient purification, TrAC Trends Anal. Chem. 132 (2020) 116051.
[52] Yang, H., S. Koza, and W. Chen *Anion-exchange chromatography for determining empty and full capsid contents in adeno-associated virus*. 2020.
[53] G. Carta, A. Jungbauer, Protein Chromatography: Process Development and Scale-Up, Wiley-VCH Verlag GmbH & Co. KGaA, 2010.
[54] D. Antos, et al., Concentration dependence of lumped mass transfer coefficients - linear versus non-linear chromatography and isocratic versus gradient operation, J. Chromatogr. A 1006 (1–2) (2003) 61–76.
[55] A. Felinger, G. Guiochon, Comparison of the kinetic models of linear chromatography, Chromatographia 60 (2004) S175–S180.
[56] S. Perveen, et al., Simulations of liquid chromatography using two-dimensional non-equilibrium lumped kinetic model with bi-Langmuir isotherm, Chem. Eng. Res. Design 181 (2022) 14–26.
[57] F. Rischawy, et al., Good modeling practice for industrial chromatography: mechanistic modeling of ion exchange chromatography of a bispecific antibody, Comput. Chem. Eng. 130 (2019) 14.
[58] L.M. Blumberg, Theory of gradient elution liquid chromatography with linear solvent strength: part 1. Migration and elution parameters of a solute band, Chromatographia 77 (1–2) (2014) 179–188.
[59] J.C. Ford, J. Ko, Comparison of methods for extracting linear solvent strength gradient parameters from gradient chromatographic data, J. Chromatogr. A 727 (1) (1996) 1–11.
[60] D. Guillarme, et al., A simple mathematical treatment for predicting linear solvent strength behavior in gradient elution: application to biomolecules, J. Sep. Sci. 45 (17) (2022) 3276–3285.
[61] M.K. Srinivasa, et al., Modifying Kohlrausch's law to describe nonaqueous electrolytes for lithium-ion batteries, ACS Appl. Mater. Interfaces 15 (51) (2023) 59296–59308.
[62] J..M. Sommer, et al., Quantification of adeno-associated virus particles and empty capsids by optical density measurement, Mol. Therapy 7 (1) (2003) 122–128.
[63] J.F. Wright, et al., Identification of factors that contribute to recombinant AAV2 particle aggregation and methods to prevent its occurrence during vector purification and formulation, Mol. Therapy 12 (1) (2005) 171–178.
[64] J. Bernaud, et al., Characterization of AAV vector particle stability at the single-capsid level, J. Biol. Phys. 44 (2) (2018) 181–194.
[65] E. Burova, E. Ioffe, Chromatographic purification of recombinant adenoviral and adeno-associated viral vectors: methods and implications, Gene Ther. 12 (1) (2005) S5–S17.